

ALMA Memo No. 529

Velocity and structure function of phase screen aloft Chajnantor

Hideharu Ishizaki and Seiichi Sakamoto
National Astronomical Observatory of Japan
Mitaka, Tokyo 181-8588, Japan

2005-06-03

Abstract

We analyzed the phase data from simultaneous measurements with the two sets of radio seeing monitors aligned in series at the ALMA site. During the one month period in summer from 1999 November 11 to December 12, the median value of the spatial phase structure function exponent deduced from the 300 m and 600 m baseline data was 0.59. The exponent independently extracted from the temporal phase structure function at the 300 m baseline was 0.62, supporting the above value obtained from the spatial phase structure function. These median values lie midway of the values for thin screen (1/3) and thick screen (5/6). No evidence for diurnal variation of the temporal phase structure function exponent was found in our data on the contrary to the previous report.

The phase screen velocity calculated from the lag time of the maximum correlation of the two sets of phase data had good correlation with the surface wind velocity at 8 m except for higher values by about 1.2. This indicates that the screen height deduced using the surface wind velocity as the screen velocity needs to be corrected upward. Provided the logarithmic wind profile and plausible roughness length ($z_0 \simeq 0.05$), the measured small ratio is understood as a reflection of small height difference of the flows, namely very low height to the phase screen (< 1 km).

1 Introduction

One of the biggest challenges to ALMA is phase calibration that is essential to realize a $0.01''$ resolution. For phase calibration and dynamic scheduling, it is important to know the nature of the phase variation at the site. In this paper we report results from the two radio seeing monitors (RSMs) aligned in series to the E-W direction, i.e., the option 2 of [1], with special emphases on the velocity and structure function of the phase screen.

2 Site and Instrumentation

In 1999 March, NAOJ redeployed the second RSM next to the first one at Pampa la Bola area (alt. = 4800 m), so that these two RSMs are in series and are aligned to the E-W direction along which the dominant wind from the west blows. Each RSM had a baseline of 300 m, with the western antenna of the eastern RSM (RSM-A) and the eastern antenna of the western RSM (RSM-B) located side-by-side (Figure 1).

All four antennas received 11.2 GHz beacon signal on Intelsat 603 (24.5° W) geostationary satellite with an azimuth of 64.5° and an elevation of 35.0° from the site. The phase differences from the two RSMs are recorded every 1 s on a PC through GPIB (Figure 2). Time stamps of

the data from the RSMs relied on the internal clock of the PC adjusted to the local civil time without summer time correction (UT - 4h). Although the absolute values of the time stamp might have errors up to several minutes, the data from the two RSMs are perfectly synchronized.

Because of the long IF cable (450 m) to the eastern antenna of RSM-A, the measurements in the dual mode were unstable, and here we report the results during the period from 1999 November 11 to December 12 when the measurements were the most stable. Note that the data are biased to summer period and that the data for the second half night are systematically missing due to the power shortage of the site testing container. Hence care must be taken when discussion of any statistical nature will be made based on the present results.

Surface wind velocity and direction were measured with a high-response anemometer atop an 8 m mast [2].

We analyzed the data based on the standard procedures adopted by the joint ALMA site testing team as described in [3]: We corrected the obtained raw phase data for the 180° ambiguity, binned every and fitted them with a second-order polynomial. We hereafter refer to the data as “phase data”.

3 Phase Structure Function

3.1 Spatial Phase Structure Function

With the configuration shown in Figure 1 and provided that the phase difference of the side-by-side antennas (A2 and B1 in Figure 1) is negligible, we can calculate the phase difference at the 600 m baseline by simple summation of the phase difference at the 300 m baselines [1].

Spatial phase structure function $D_\phi(\rho)$ is defined as,

$$D_\phi(\rho) \equiv \langle (\phi(\rho_0) - \phi(\rho_0 + \rho))^2 \rangle \simeq \sigma_\phi^2(\rho), \quad (1)$$

where ρ is a baseline length, ρ_0 is the reference baseline length (= 300 m), and $\sigma_\phi(\rho)$ is an rms phase measured at a baseline length ρ [3]. Here we fit the spatial phase structure function, or the mean square phase at different baseline length, with a power law with an exponent α ,

$$\sigma_\phi(\rho) = \sigma_\phi(\rho_0) \left(\frac{\rho}{\rho_0} \right)^\alpha. \quad (2)$$

For a set of data taken with the 300 m¹ and 600 m baselines, the exponent α in this baseline range is calculated by,

$$\alpha = \log_2 \left(\frac{\sigma_\phi(600 \text{ m})}{\sigma_\phi(300 \text{ m})} \right). \quad (3)$$

Plot of the exponent α as a function of local time in Figure 3 exhibits, however, large scatter that prevents us from any robust arguments on diurnal variation. Overall statistics in Figure 4, though biased, shows that the median value of the exponent α is 0.59, which is intermediate between the values for thin screen (1/3) and thick screen (5/6).

3.2 Temporal Phase Structure Function

Temporal phase structure function $\bar{D}_\phi(\tau)$ is defined as,

$$\bar{D}_\phi(\tau) \equiv \langle (\phi(t) - \phi(t + \tau))^2 \rangle, \quad (4)$$

¹Here we only used the 300 m baseline data taken with RSM-B because of the lower instrumental phase noise compared with RSM-A.

with a time interval τ [4]. Under the frozen phase screen model, spatial phase structure function is transformed into temporal phase structure function with the screen velocity as,

$$\bar{D}_\phi(\tau) = D_\phi(\rho) \Big|_{\rho=v_s\tau}. \quad (5)$$

Example of the temporal phase structure function at the 300 m baseline is shown in Figure 5. Temporal phase structure function was fitted with two lines – shorter timescale exponential component and dc component at larger timescale range – and the “corner time” t_c was calculated as their crossing point in a manner similar to that described in [3]. Again we only used the 300 m baseline data taken with RSM-B.

Here we fit the short timescale part of the temporal phase structure function with a power law with an exponent β ,

$$\bar{D}_\phi(\tau) \propto \left(\frac{\tau}{\tau_0}\right)^\beta; \tau < t_c. \quad (6)$$

Under the frozen phase screen model, β should be equal to 2α .

Obviously it is interesting to test if the exponent β of the power law fit to the temporal structure function agrees with the exponent (2α) of the power law fit to the spatial phase structure function, and we thus plotted $\beta/2$ in Figures 6 and 7 as analogies with Figures 3 and 4. However, because of the large scatter of the spatial phase structure function exponent, it is difficult to judge if the spatial and temporal phase structure function exponents are consistent.

As for the temporal phase structure function exponent, we can test if the current results is consistent with the previous results by Delgado & Nyman (2001) who claimed, diurnal variation of the temporal phase structure function exponent based on the data taken with two water vapor radiometers (WVRs) on 1999 November 15. The present results do not support the previous arguments — the temporal phase structure function exponent does not have diurnal variation from $\simeq 1/3$ (thin screen) during UT – 4h = 20h–8h to $\simeq 5/6$ (thick screen) during 11h–16h [4]. Judging from their Figure 9, we suspect that their conclusion was affected by artifacts due to the instrumental noise that ended up systematic underestimation of the exponent under low phase noise conditions. Since neither their data nor ours are sufficient for statistical use, extensive study should be carried out with more complete datasets to close this issue.

4 Phase Screen Velocity

With two sets of RSMs of identical baseline length aligned to E-W, we can calculate the E-W component of the phase screen velocity v_s as,

$$v_s = L/t_1, \quad (7)$$

with the separation of the RSMs L ($= 300$ m) and the lag time t_1 of the maximum cross correlation of the phase data obtained with the two RSMs. Figure 8 is an example of plots of cross correlation function for different time ranges that demonstrates how the lag time was determined. Negative velocity means a flow from the west.

Although the data may be biased, the deduced histogram and cumulative distribution of the E-W component of the screen velocity (Figure 9) illustrates that the screen moves from west for most of the time, and there exists a certain amount of time when anomalously high ($> 100 \text{ m s}^{-1}$) screen velocity is observed.

Although the extracted values in the high velocity end are badly quantized because of the 1 s sampling interval (remind v_s becomes -300 m s^{-1} for $t_1 = -1$ s and -150 m s^{-1} for -2 s), the existence of such high velocity components is robust. Suspected artifact due to the N-S motion of the phase screen is not the case because of the lack of its counterpart in positive velocity and because of the presence of a gap between $t_1 = -4$ to -6 s.

From the time series of the phase data taken with the two RSMs during the period with fast-traveling component (Figure 10), it is clear that this fast-traveling component corresponds to “anomalous fast phase fluctuation” [5]. We will defer further analysis of the phase data from this aspect to a forthcoming paper.

5 Height to Phase Screen

The E-W components of the screen velocity and the surface wind velocity exhibit a good relationship as demonstrated in Figure 11. A closer look, however, reveals a quantitative difference between these velocities. In Figure 12, correlation of the E-W component of the screen velocity v_s and that of the wind velocity $v_w(z)$ was plotted separately for the day (UT - 4h = 9:00–18:00) and night (18:00–9:00). No significant day-to-night difference was found, and the best fit to all of the data with $-99 \text{ m s}^{-1} < v_s < 0 \text{ m s}^{-1}$ and $v_w < 0 \text{ m s}^{-1}$ was $v_s = 1.2 v_w(8 \text{ m})$ with a correlation coefficient of 0.93. This good correlation suggests that the phase screen is within the atmospheric boundary layer.

The measured ratio of the screen velocity and surface wind velocity appears significantly different from those reported earlier with the wind data taken with a weather station atop a 3 m mast ($v_s/v_w(3 \text{ m}) \sim 2$; [4, 6]). However, because $v_w(8 \text{ m})$ can be larger than $v_w(3 \text{ m})$ by a few 10% [2], the measured ratio of $v_s/v_w(8 \text{ m}) = 1.2$ may be consistent with the previous study [4] and support their argument that the quantitative value of the height to the phase screen in [7] obtained on assumption that $v_s/v_w(3 \text{ m}) = 1$ should be scaled by a certain factor (1.2 in this case).

The above difference in screen velocity and surface wind velocities may reflect the difference in the heights of the flows, and these results may be also used to hint the height to the screen, provided a logarithmic profile of the surface wind velocity $\bar{v}(z)$,

$$\bar{v}(z) = \frac{v^*}{k} \ln \left(\frac{z}{z_0} \right), \quad (8)$$

where v^* is the friction velocity, k is the von Kármán constant ($\simeq 0.4$), and z_0 is the roughness length. The screen velocity is then extracted from the velocity ratio v_s/v_w and the height of the wind measurement z_w ,

$$z_s = (z_w)^{v_s/v_w} (z_0)^{1-v_s/v_w}, \quad (9)$$

as plotted in Figure 13. By assuming plausible roughness length ($z_0 \simeq 0.05$) at the site, the measured small ratio ($\simeq 1.2$) implies very low height to the phase screen ($< 1 \text{ km}$) for most of the period.

6 Time Evolution of Phase Screen

The cross correlation function of the RSM-A and RSM-B phase data shown in Figure 14 exhibits positive correlation with the screen velocity. This is a possible reflection of the time evolution of the phase screen. The median value of the correlation function of the RSM-A and RSM-B phase data becomes 0.5 when the screen velocity was 11 m s^{-1} , indicating that the evolution timescale, or the timescale for half decorrelation, of the phase screen was 27 s in 1999 November–December.

7 Summary and Future Work

We analyzed the phase data from simultaneous measurements with the two sets of radio seeing monitors aligned in series at the ALMA site. During the one month period in the austral summer

from 1999 November 11 to December 12, the median value of the spatial phase structure function exponent was 0.59. The exponent deduced from the temporal phase structure function was 0.62, supporting the value obtained from the spatial phase structure function. On the contrary to the previous arguments by Delgado & Nyman (2001) who analyzed the data taken with two WVRs on 1999 November 15, no evidence for diurnal variation of the temporal phase structure function exponent from $\simeq 1/3$ (thin screen) during UT - 4h = 20h-8h to $\simeq 5/6$ (thick screen) during 11h-16h was found in our data taken during the same period. We suspect that their conclusion was affected by the artifacts due to the instrumental noise that ended up systematic underestimation of the exponent under low phase noise conditions. Extensive study should be carried out with more complete datasets for diurnal and seasonal variation of the phase structure function exponent.

Velocity of the phase screen calculated from the lag time that gives the maximum cross correlation of the two phase data had good correlation with the surface wind velocity measured at 8 m, with higher values by about 1.2. This supports the argument by Delgado & Nyman (2001) that the quantitative value of the height to the phase screen in Robson et al. (2001) obtained on assumption that $v_s/v_w(3\text{ m}) = 1$ should be scaled by a certain factor (1.2 in this case). The difference between the screen velocity and surface wind velocity may be also understood in terms of their height differences and provides independent information on the screen height. Based on the assumptions of the logarithmic wind profile and plausible roughness length ($z_0 \simeq 0.05$) at the site, the measured small ratio implies very low height to the phase screen ($< 1\text{ km}$).

Evolution timescale of the phase screen was estimated from the timescale of half de-correlation, and its median value was 27 s with large scatters.

Phenomenon known as “anomalous fast phase fluctuation” [5] was observed as the fast-traveling component over the RSMs. Analysis of this phenomenon will be presented in a separate paper.

We thank the ALMA site testing team who jointly established and maintained the instruments and collected the data in the altiplano.

References

- [1] Holdaway, M. A., & Radford, S. J. E. 1998, “Options for placement of a second site test interferometer on Chajnantor”, ALMA Memo 196
- [2] Sakamoto, S., Ishizaki, H., & Kohno, K. 2004, “Wind power spectrum near Chajnantor”, ALMA Memo 500
- [3] Holdaway, M. A., Radford, S. J. E., Owen, F. N., & Foster, S. M. 1995, “Data processing for site test interferometers”, ALMA Memo 129
- [4] Delgado, G., & Nyman, L.-Å. 2001, “Velocity of the effective turbulence layer at Chajnantor estimated from 183 GHz measurements”, ALMA Memo 363
- [5] Hales, S., Hills, R., Robson, Y., Richer, J., Delgado, G., Otárola, A., & Radford, S. J. E. 2003, “Investigation of anomalous fast phase fluctuations in the site-test interferometer data from Chajnantor”, ALMA Memo 459
- [6] Holdaway, M. A. 1995, “Velocity of wind aloft from site testing interferometer data”, ALMA Memo 130
- [7] Robson, Y., Hills, R., Richer, J., Delgado, G., Nyman, L.-Å., Otárola, A., Radford, S. J. E. 2001, “Phase fluctuation at the ALMA site and the height of the turbulent layer”, ALMA Memo 345

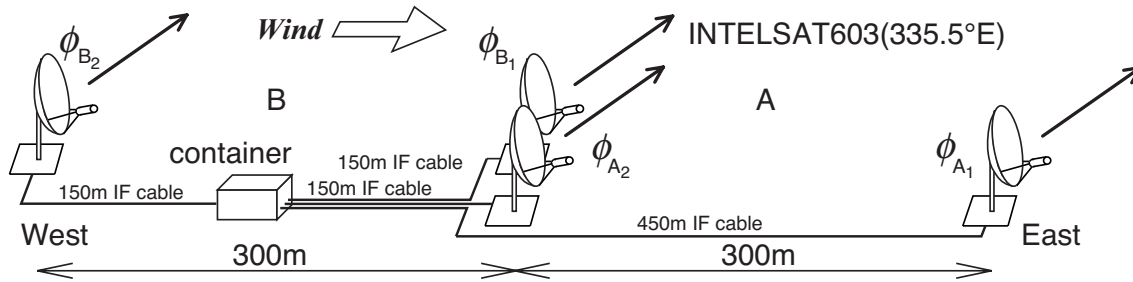


Figure 1: Configuration of the two radio seeing monitors (RSMs) deployed at Pampa la Bola along the E-W direction.

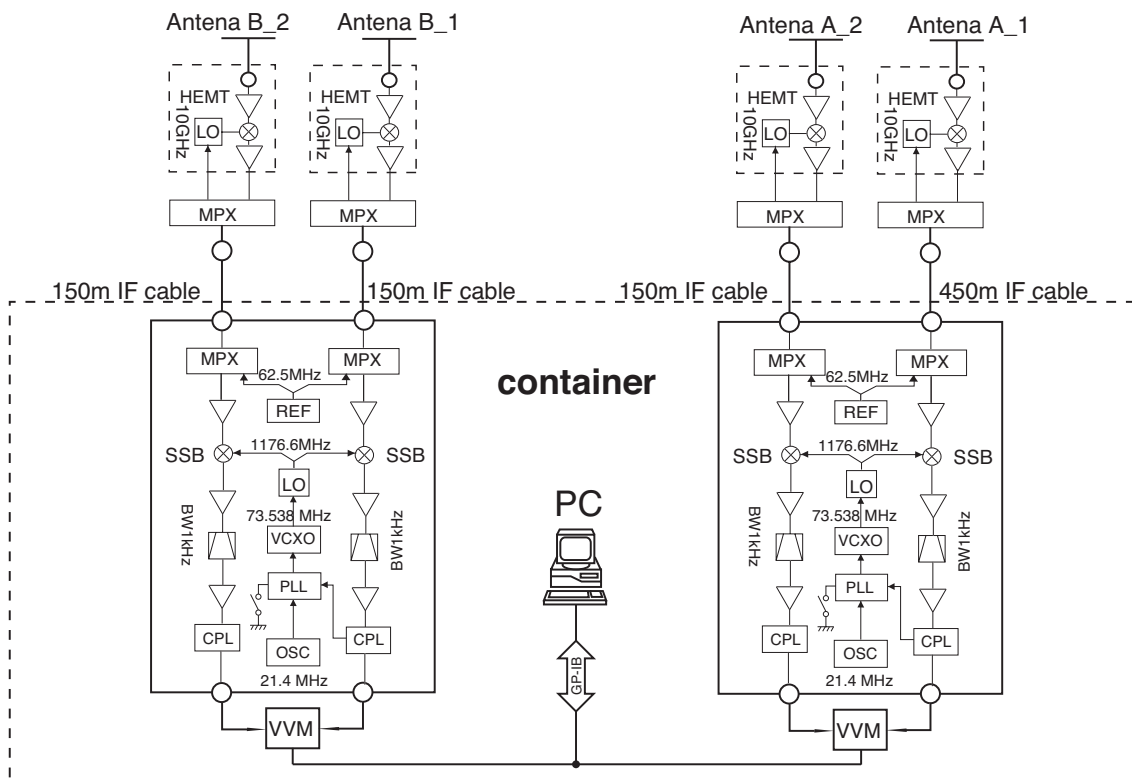


Figure 2: Block diagram of the two RSMs.

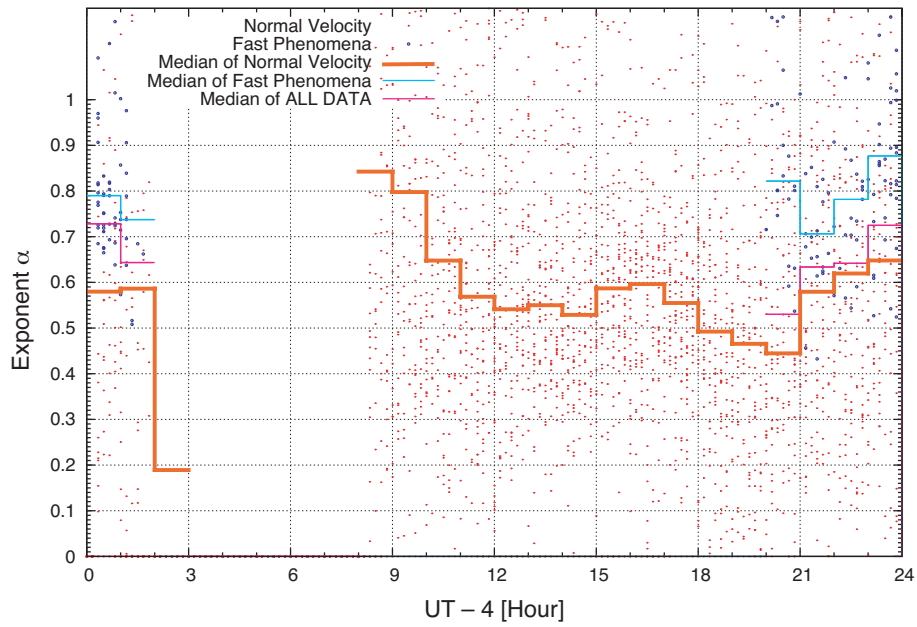


Figure 3: Plot of the exponent α of the spatial phase structure function (*dots*) and their median values (*lines*) as a function of local time. Each point corresponds to the exponent α calculated every 10 min, with red dots for the data under regular conditions and blue dots under the onset of the anomalous fast phase fluctuation [5].

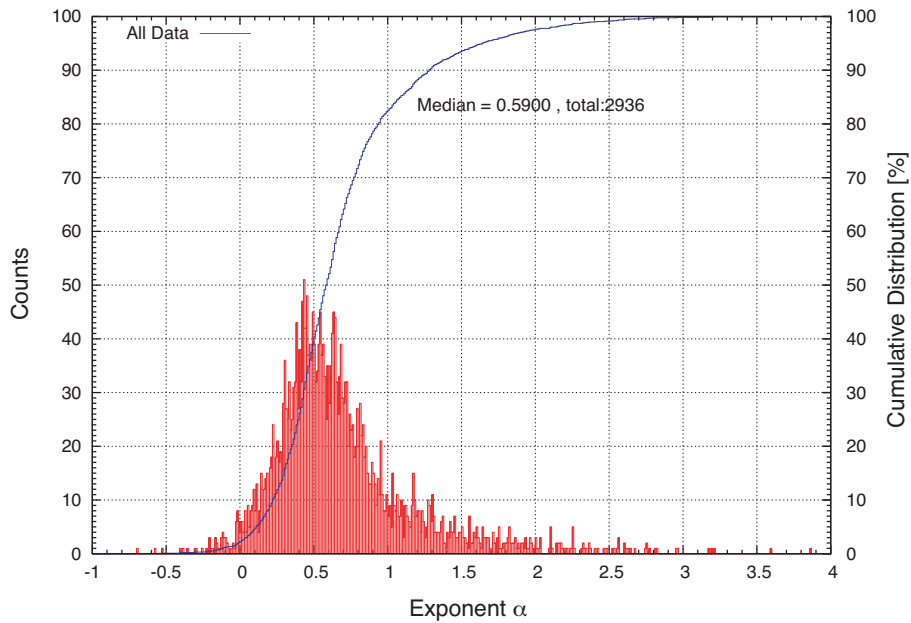


Figure 4: Histogram and cumulative distribution of the exponent α of the spatial phase structure function.

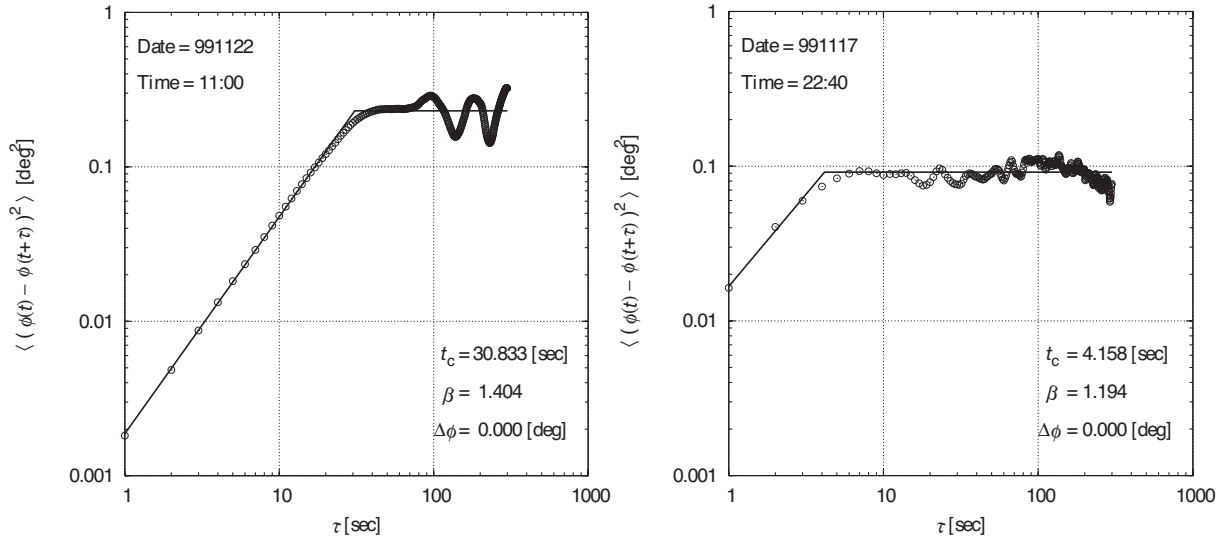


Figure 5: (a: *left*) An example of the temporal phase structure function on 1999 November 22, 11:00–11:10 (UT – 4h). Open circles indicate measured $\bar{D}_\phi(\tau)$, and lines indicate the best fit of $\bar{D}_\phi(\tau) - \Delta\phi$. Indicated in the figure, t_c is the corner time, β is the exponent of the short timescale part, $\Delta\phi$ is the instrumental phase noise, obtained by the fitting procedures. (b: *right*) Same as (a) but during the period when the anomalous fast phase fluctuation was observed (1999 November 17, 22:40–22:50).

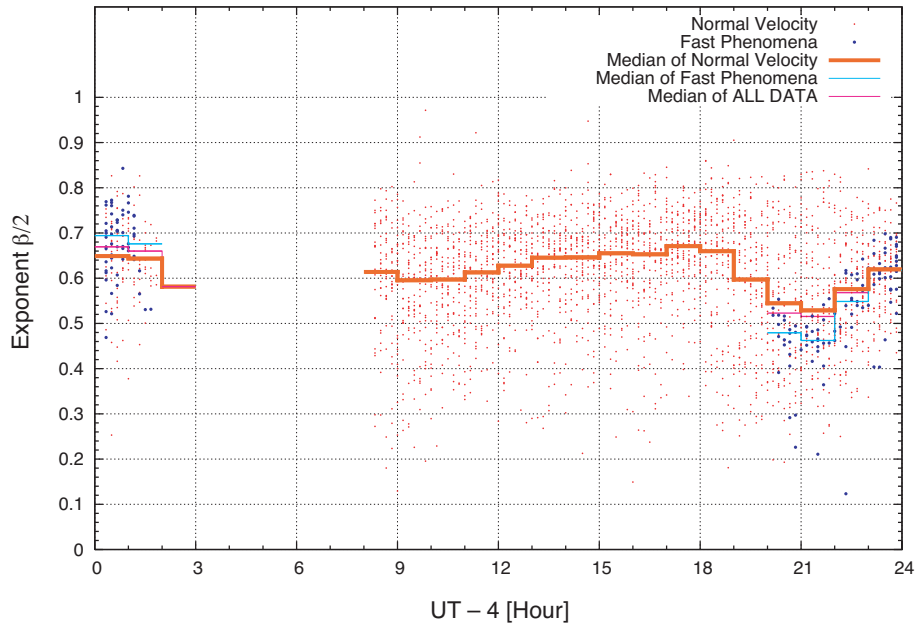


Figure 6: Plot of the exponent $\beta/2$ of the temporal phase structure function (*dots*) and their median values (*lines*) as a function of local time. Each point corresponds to the exponent α calculated every 10 min, with the ones coded in red for the data under regular conditions, and those in blue for the data under the onset of the anomalous fast phase fluctuation.

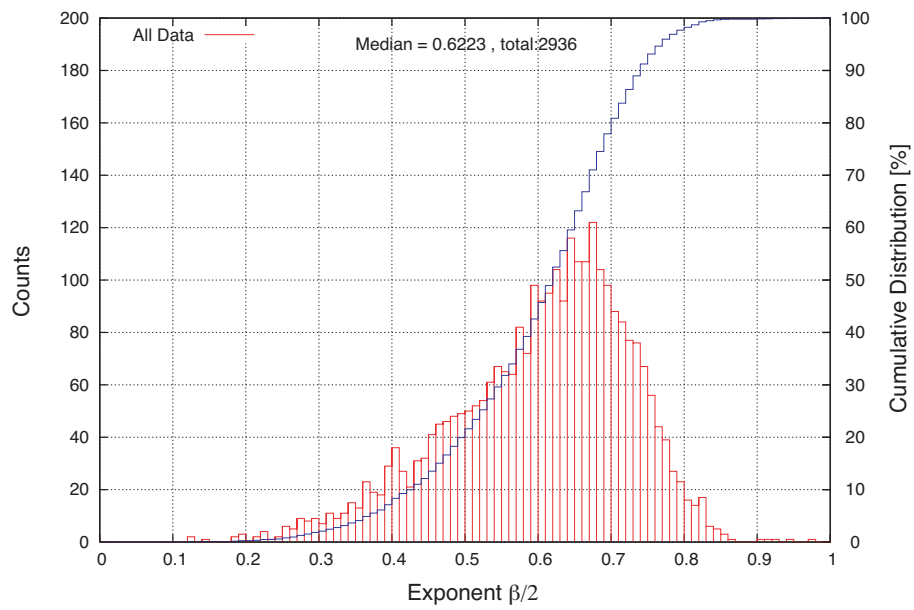


Figure 7: Histogram and cumulative distribution of the exponent $\beta/2$ of the temporal phase structure function.

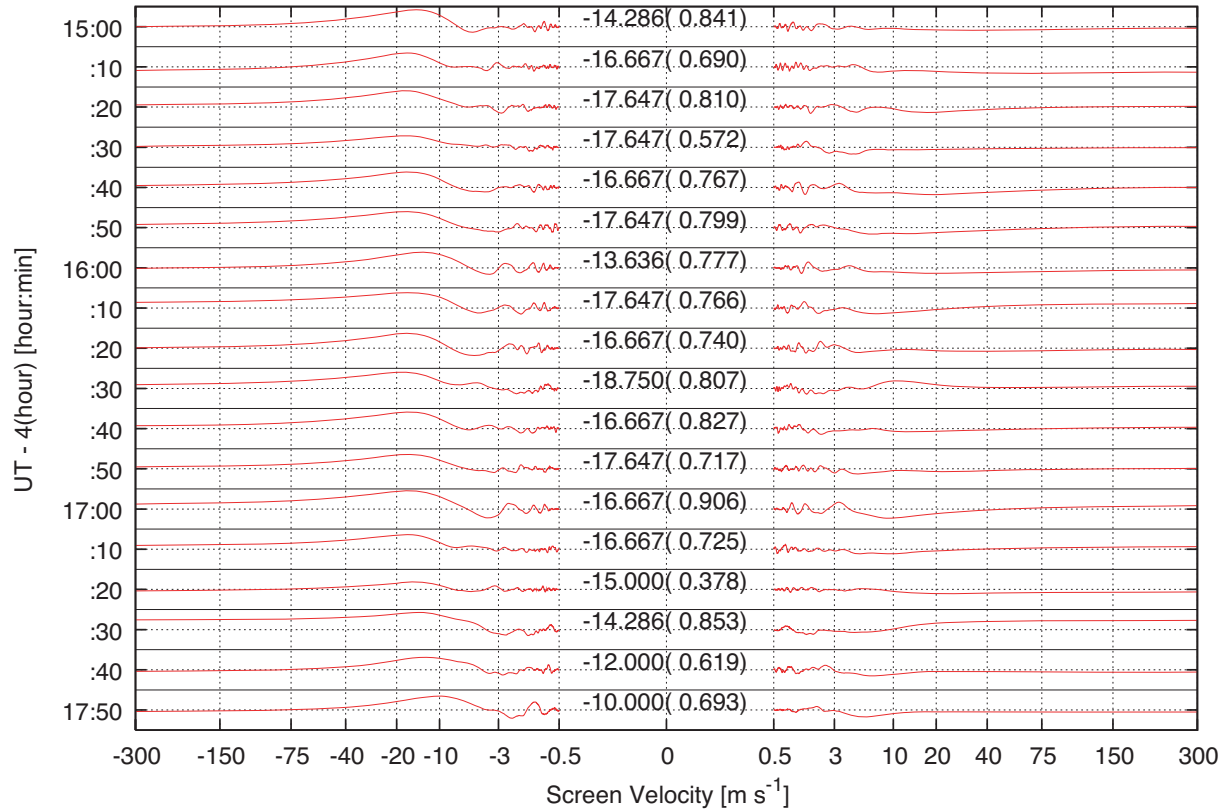


Figure 8: Examples of cross correlation function for different time ranges on 1999 November 16. Full range of the vertical axis of each panel is from -1 to $+1$. Each number in the center of the plot indicates the velocity at the maximum correlation, with corresponding maximum correlation value in the parentheses.

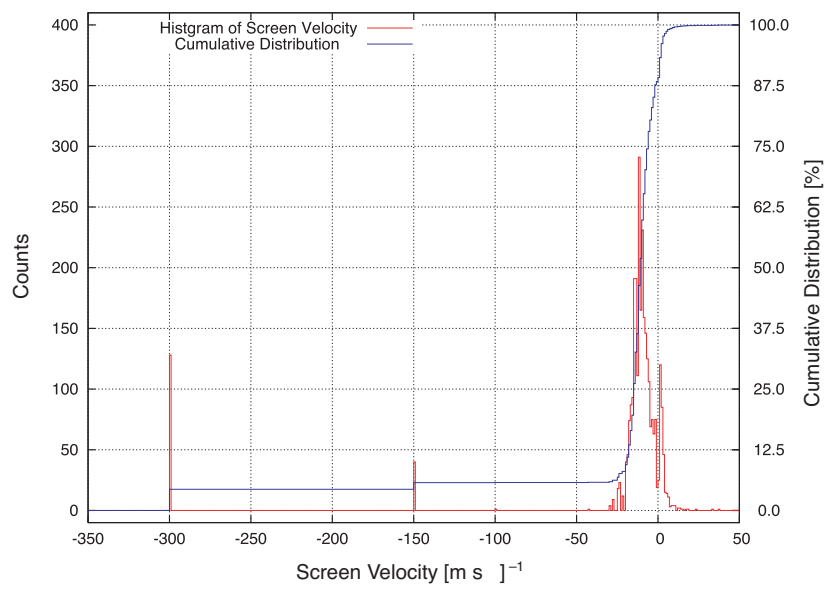


Figure 9: Histogram and cumulative distribution of the E-W component of the screen velocity.

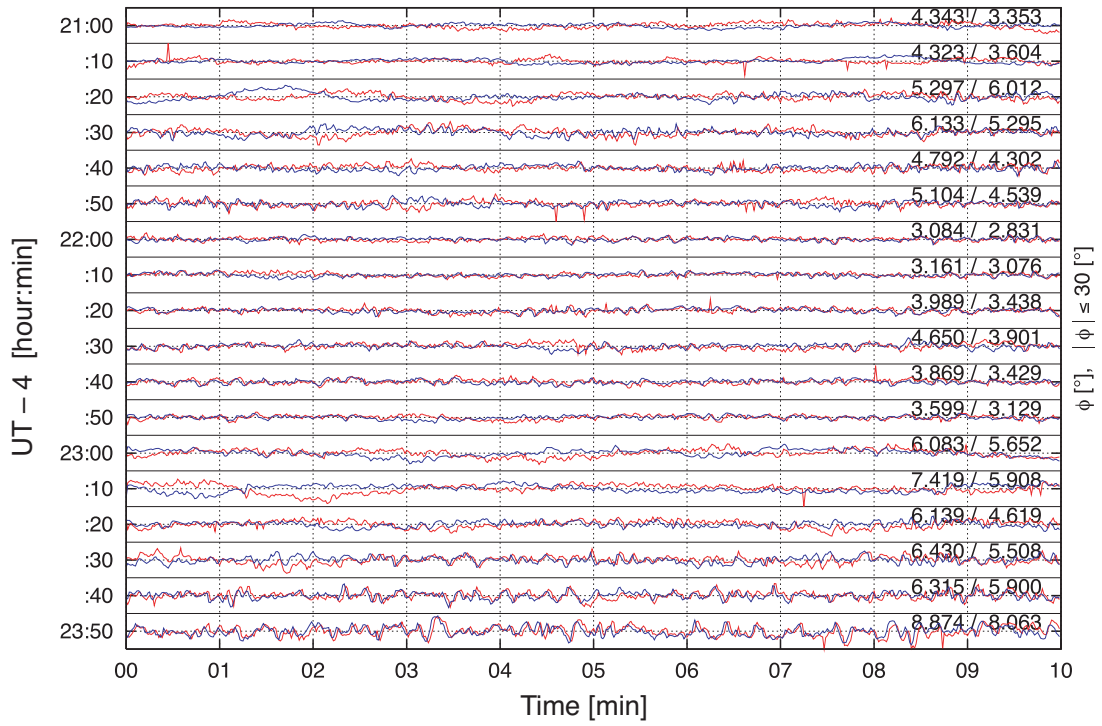


Figure 10: Time series of the phase data taken with RSM-A (*red*) and RSM-B (*blue*) during the night on 1999 November 17 when the anomalous fast phase fluctuation was observed. Numbers shown in the right hand side of each panel indicate rms phase of RSM-A and RSM-B.

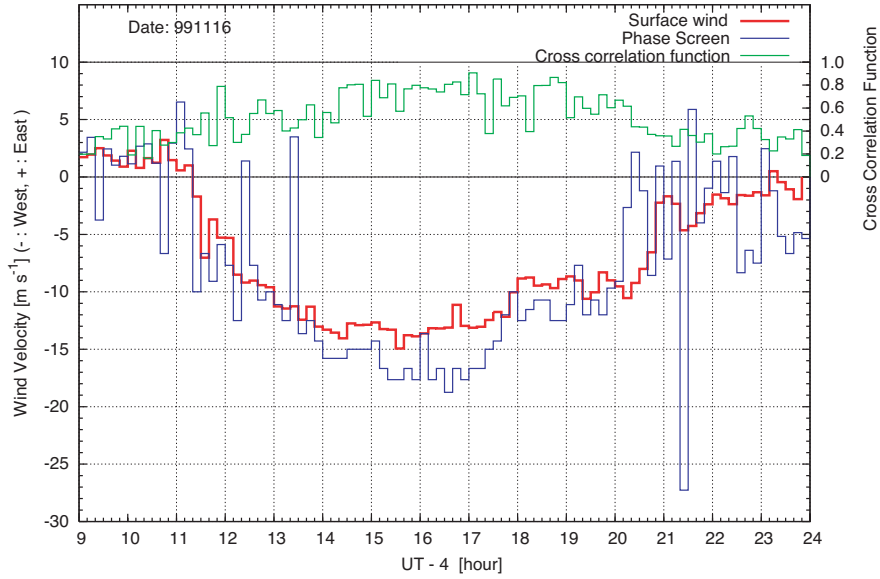


Figure 11: Time series of the E-W component of the screen velocity (*blue*) and that of the surface wind velocity (*red*) on 1999 November 16. Cross correlation function of the RSM-A and RSM-B phase data (*green*) is also shown.

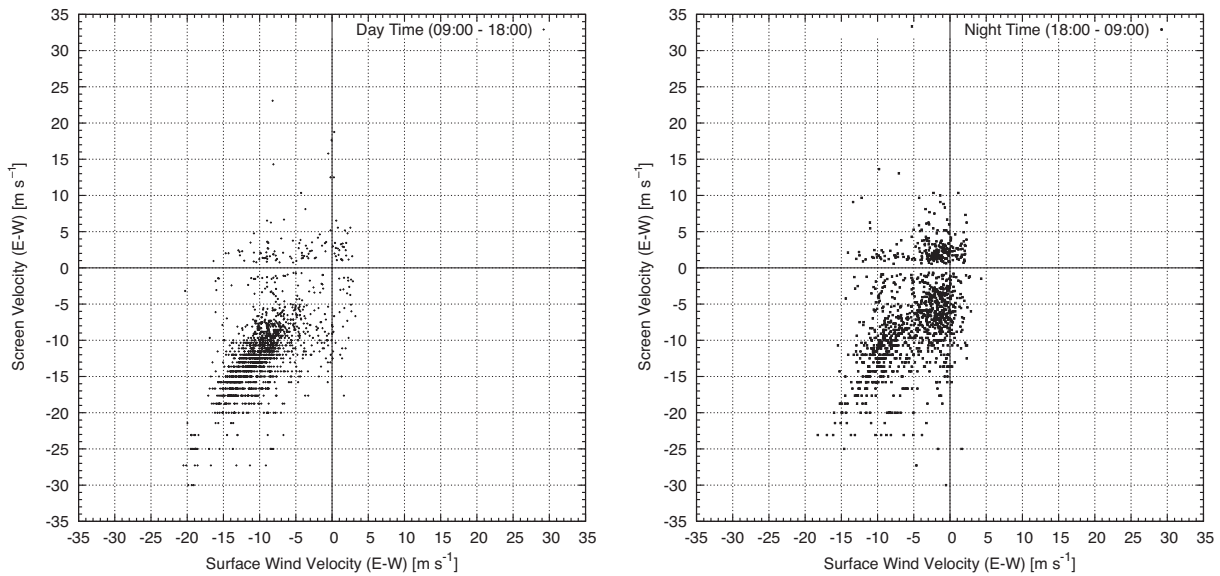


Figure 12: Correlation of the E-W component of the screen velocity and that of the wind velocity during the daytime (UT - 4h = 9:00–18:00; *left*) and the nighttime (18:00–9:00; *right*).

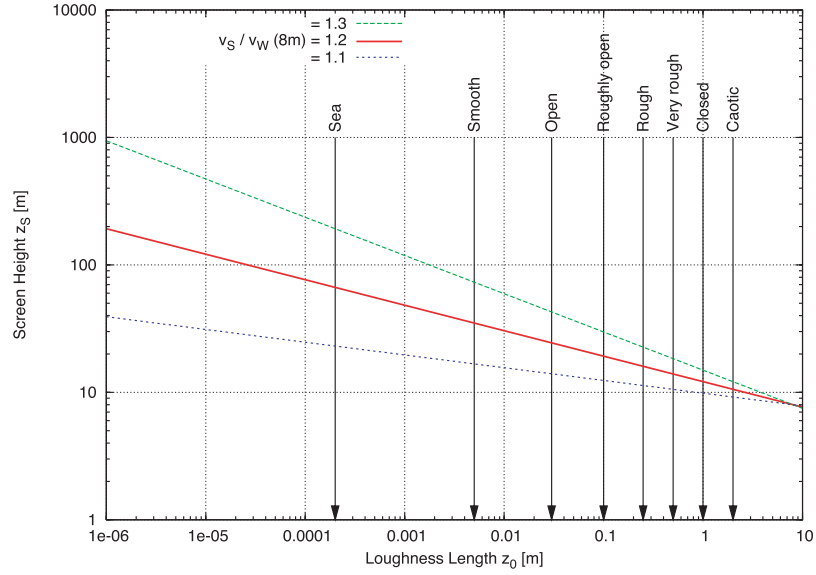


Figure 13: Screen height extracted from measured velocity difference of the phase screen and surface wind at 8 m based on the logarithmic wind velocity profile.

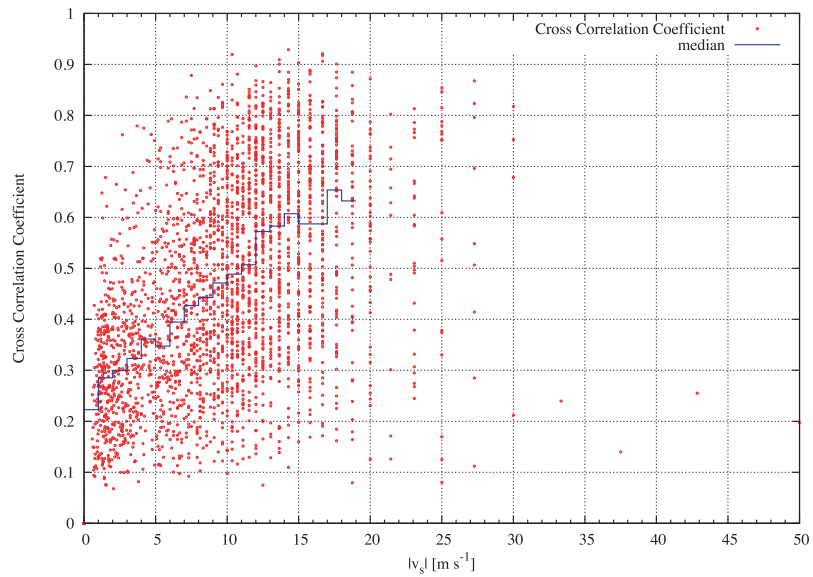


Figure 14: Correlation between the E-W component of the screen velocity and the cross correlation function of the RSM-A and RSM-B phase data.